

Wafer-Scale Fabrication of Self-Catalyzed 1.7 eV GaAsP Core–Shell Nanowire Photocathode on Silicon Substrates

Jiang Wu,^{*,†} Yanbo Li,^{*,‡} Jun Kubota,[‡] Kazunari Domen,[‡] Martin Aagesen,[§] Thomas Ward,^{||} Ana Sanchez,^{||} Richard Beanland,^{||} Yunyan Zhang,[†] Mingchu Tang,[†] Sabina Hatch,[†] Alwyn Seeds,[†] and Huiyun Liu^{*,†}

[†]Department of Electronic and Electrical Engineering, University College London, Torrington Place, London WC1E 7JE, United Kingdom

[‡]Department of Chemical System Engineering, The University of Tokyo, 7-3-1 Hongo, Bunkyo-ku, Tokyo 113-8656, Japan

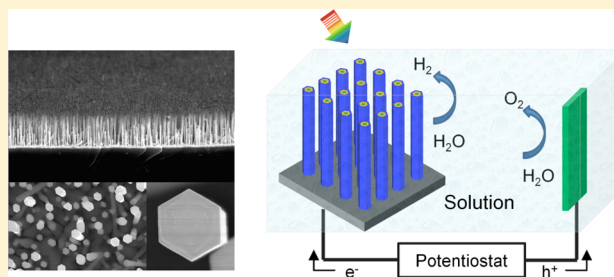
[§]Gasp Solar ApS, Gregersensvej 7, Taastrup DK-2630, Denmark

^{||}Department of Physics, University of Warwick, Coventry CV4 7AL, United Kingdom

Supporting Information

ABSTRACT: We present the wafer-scale fabrication of self-catalyzed p–n homojunction 1.7 eV GaAsP core–shell nanowire photocathodes grown on silicon substrates by molecular beam epitaxy with the incorporation of Pt nanoparticles as hydrogen evolution cocatalysts. Under AM 1.5G illumination, the GaAsP nanowire photocathode yielded a photocurrent density of 4.5 mA/cm² at 0 V versus a reversible hydrogen electrode and a solar-to-hydrogen conversion efficiency of 0.5%, which are much higher than the values previously reported for wafer-scale III–V nanowire photocathodes. In addition, GaAsP has been found to be more resistant to photocorrosion than InGaP. These results open up a new approach to develop efficient tandem photoelectrochemical devices via fabricating GaAsP nanowires on a silicon platform.

KEYWORDS: Nanowire, hydrogen, water splitting, GaAsP, photocathode, self-catalyzed, molecular beam epitaxy



The global energy and environmental crisis requires increasingly urgent solutions to develop sustainable energy technologies. Renewable energy such as solar energy is a promising power source relative to fossil fuels.¹ However, the intermittency of renewable energy is a great challenge to current energy systems. The storage of harvested renewable energy in chemical form, mimicking the photosynthesis of plants, is considered as a promising option in the deployment of renewable energy technologies.² Hydrogen, one of the simplest chemical compounds in nature, possesses attractive properties as a green energy carrier such as high energy density and benign environmental impact.³ Hydrogen generated by solar energy through direct splitting of water is thus considered as the fuel of the future. Despite intensive research activities stretching back to the 1970s, the efficiency of direct conversion of solar energy to hydrogen remains a big challenge.⁴ High-efficiency photoelectrochemical water splitting requires photoelectrodes that can provide at least the thermodynamic potential of 1.23 V for water splitting and can convert a large portion of energy from the solar spectrum.^{5,6} Wide bandgap semiconductors, such as TiO₂, have been widely investigated due to their high photocatalytic activity and superior photochemical stability.^{7,8} However, the photoelectrodes made from wide bandgap materials (~3.0 eV) only absorb a rather small part of the solar spectrum setting an upper solar-to-hydrogen

(STH) efficiency limit of only ~2%.^{9,10} The bandgap of ideal semiconductor materials for single-bandgap photoelectrode should be large enough (>1.6 eV) to split water and, at the same time, small enough (<2.4 eV) to absorb a wide range of the solar spectrum.⁹ For example, a bandgap of 2.0 eV for a single semiconductor material has an optimum theoretical STH efficiency of 17.4%.¹¹ While the semiconductors with a smaller bandgap offer substantial solar spectrum coverage and potentially high STH conversion efficiency, the stability of these materials presents a major challenge in water splitting.^{12–14}

The dilemma of low STH efficiency for single-bandgap systems can be addressed by the use of two absorbing semiconductor materials, in which the wider bandgap material is placed on top for photoelectrodes and absorbing the short wavelength, while a smaller bandgap material is placed behind the wider bandgap one to absorb the long-wavelength solar spectrum. This will enhance the solar spectrum coverage dramatically and hence give a potentially higher STH efficiency. The highest STH efficiency of 28% was theoretically predicted for dual-bandgap systems by taking losses of ~0.8 eV into

Received: January 15, 2014

Revised: March 12, 2014

Published: March 28, 2014

consideration.¹¹ Due to the material availability for two-bandgap systems, the highest theoretical STH efficiency for practical tandem photoelectrodes will be a 27.0% by the combination of 1.7 eV III–V and 1.1 eV silicon absorption.¹¹ However, the thermal and lattice mismatch between III–V bulk and silicon substrates have hindered the effective implantation of tandem 1.7 eV/1.1 eV III–V/Si tandem photoelectrodes.

On the other hand, the bandgap of GaAsP materials can be tuned from 1.42 to 2.26 eV, which is highly desired for water splitting. However, there has been no report on photoelectrodes based on GaAsP materials due to the lack of lattice-matched substrates. GaAsP nanowires have recently been demonstrated as a promising materials system for high-efficiency photovoltaic cells.^{15–17} Thanks to the one-dimensional geometry and small footprint of the nanowires, the stress induced by the lattice and thermal mismatch can be accommodated by elastic relaxation.^{18,19} In addition, by introducing a core–shell geometry, it is possible to create a radial p–n nanodiode in self-catalyzed nanowires that greatly enhances the light absorption and charge-separation efficiency.^{20–22} The direct assembly of GaAsP nanowires on Si substrates also makes a leap in cost reduction possible. Here we demonstrate a photocathode based on self-catalyzed GaAsP semiconductor nanowires monolithically grown on silicon substrates by solid-source molecular beam epitaxy (MBE). The bandgap of the GaAsP nanowires was engineered to the optimized energy gap of the top photoelectrode for a tandem cell at 1.7 eV via controlled phosphor incorporation.²³ A p–n GaAsP homojunction geometry was adopted to suppress carrier recombination and enhance charge transport.^{24–29} Direct self-catalyzed uniform ternary GaAsP nanowire arrays across an entire Si(111) wafer have been achieved, yielding a STH conversion efficiency of about 0.5%, which is higher than the values previously reported for the self-catalyzed III–V nanowires photoelectrodes prepared on wafer-scale.^{8,30} The STH efficiency should be further enhanced by the optimization of GaAsP nanowires and the combination of silicon junction to absorb long-wavelength solar spectrum. These GaAsP core–shell nanowires provide a new approach for developing efficient photocathodes for water splitting.

Self-catalyzed GaAsP nanowires were grown by solid-source III–V MBE directly on p-type Si(111) substrates. The fabrication of GaAsP nanowires was first carried out by a Ga droplet assisted VLS growth mechanism. The substrate temperature was kept at about 640 °C measured by a pyrometer for Ga-assisted nanowires growth. Be was supplied to form a p-type GaAsP nanowire core. After growth of the nanowire cores by VLS growth mechanism for about 1 h, the Ga droplets were crystallized into GaAsP by closing the Ga shutter and supplying As and P with beam equivalent pressures of 6.9×10^{-6} Torr and 3.1×10^{-6} Torr, respectively. Sequentially, the core growth was carried out at substrate temperatures between 460 and 470 °C. During the nanowire shell growth, Be and Si dopants were provided separately to form a p–n homojunction. Scanning electron microscopy (SEM) measurements of the nanowires were performed with a Zeiss XB 1540 FIB/SEM system. Photoluminescence was measured under excitation from a 532 nm diode-pumped solid-state laser. A Newport monochromator with dual grating was used to disperse the emission, which was then detected by a Si detector. TEM analysis was performed on JEOL 2100 and JEOL ARM200F microscopes operating at 200 kV. Compositional analysis using energy-dispersive X-ray spectrometry was

performed using Oxford Instruments 40 mm² SDD EDX detectors.

The epitaxial growth of the radial GaAsP homojunction nanowires is illustrated in Figure 1. The growth of the GaAsP

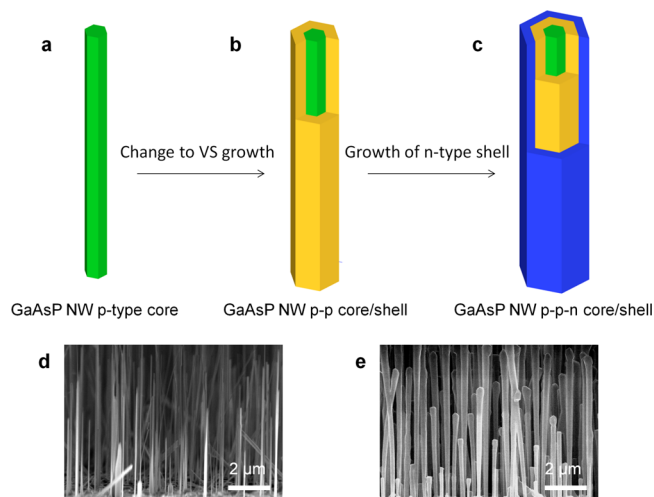


Figure 1. Schematic illustration of the nanowires assembly: (a) the self-catalyzed GaAsP nanowires with Be doping grown by the VLS mechanism, (b) the growth of p-type GaAsP shell by the VS mechanism, and (c) the growth of n-type GaAsP shell by the VS mechanism to form GaAsP p–n homojunction. (d) Side-view SEM image of p-type GaAsP nanowires grown by VLS mechanism. (e) Side-view SEM image of GaAsP p–n homojunction nanowires.

radial homojunction nanowires started with a Be doped GaAsP core prepared by the vapor–liquid–solid (VLS) growth mechanism (Figure 1a). The substrate temperature and V/III and As/P flux ratios were adjusted to the optimized growth conditions for 1.7 eV GaAsP nanowires. These self-catalyzed core nanowires are about 50–100 nm in diameter measured from SEM (Figure 1d). After the p-type core was grown by the VLS mechanism, the nanowire growth was switched from VLS to vapor–solid (VS) epitaxial growth mechanism (Figure 1b) and a p-type shell growth. Over the p-type shell, an n-type shell with silicon dopants was also grown by the VS growth mechanism to finish the structure (Figure 1c,e).^{16,23}

Figure 2 shows the detailed structural and optical properties of the self-assembled p–n core–shell GaAsP homojunction nanowires. Although selective-area epitaxy is widely used for the growth of uniform well-aligned III–V nanowires, the nanohole patterns are generally fabricated via top-down techniques such as electron beam lithography, which is not efficient and cost-effective for fabrication of nanomaterials on a large scale.^{31,32} On the other hand, the self-catalyzed growth can result in nanowires in good uniformity on a wafer scale (Figure S1 of the Supporting Information). The SEM image in Figure 2a shows the SEM images of vertically oriented arrays of self-catalyzed GaAsP nanowires. After shell growth, the nanowires are about 10 μm in length and 300 nm in diameter (Figure 2a). The areal density of the nanowires is estimated to be $\sim 1.8 \times 10^8$ cm⁻² from SEM images (Figure S2 of the Supporting Information), which corresponds to a nanowire areal fraction of only about 13%. TEM images (Figure 2b) show that the nanowires are predominantly in zinc blende crystal phase with some rotational twins. The crystal quality plays a critical role in the performance of photoelectrodes because stacking fault defects typically observed in self-

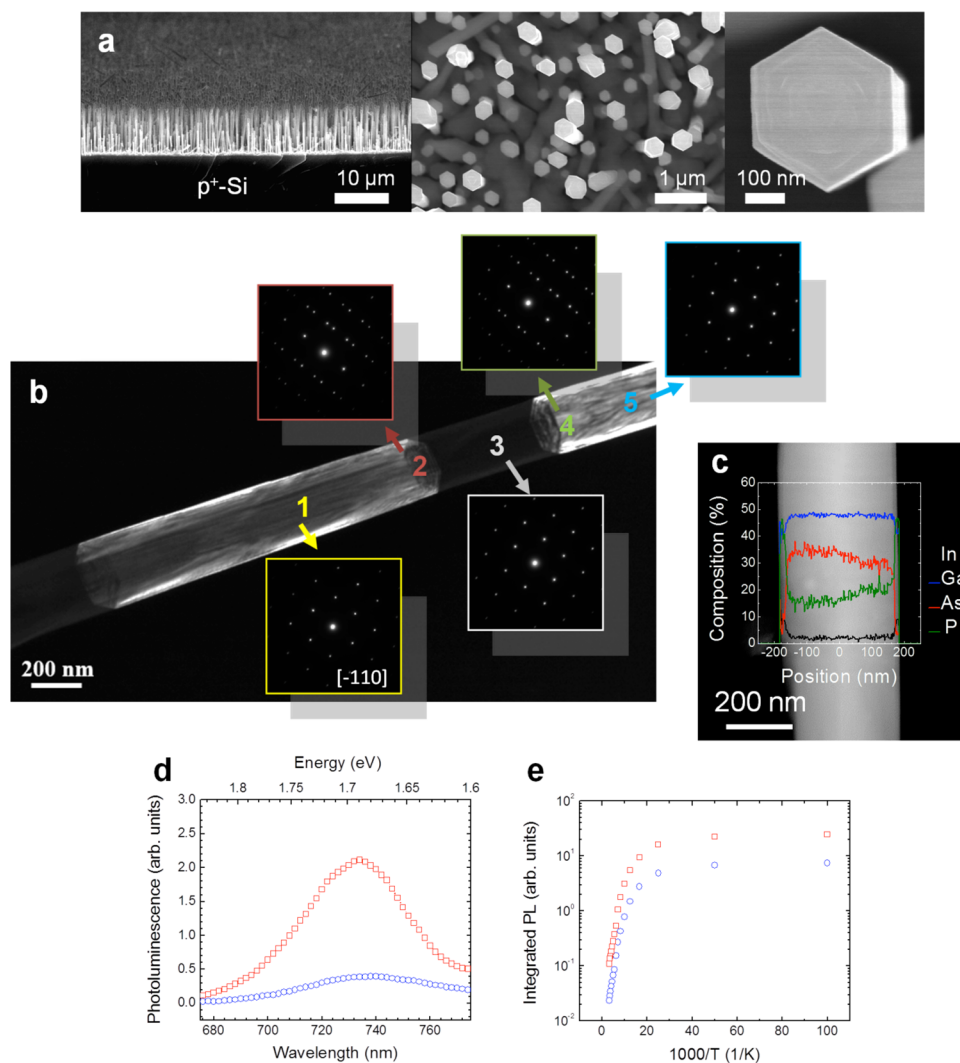


Figure 2. (a) Low-magnification side-view and top-view and high-magnification top-view SEM images of vertically orientated GaAsP p–n homojunction nanowires grown onto a p^+ -Si (111) substrate. (b) Dark field TEM images and diffraction patterns taken in different positions of a GaAsP p–n homojunction nanowire. (c) Line element mapping image of a GaAsP p–n homojunction nanowire across the radial axis. The element composition is normalized to the nanowire thickness. (d) Room temperature PL of GaAsP nanowires with (red open square) and without (blue open circle) an InGaP passivation layer. (e) Integrated PL intensity of GaAsP nanowires with (red open square) and without (blue open circle) an InGaP passivation layer as a function of temperature.

assembled nanowires are detrimental to charge transport in these nanowires. It has been shown that major differences between zinc blende and wurtzite nuclei exist for the interfacial energy.³³ The P/As ratio and V/III ratio are critical parameters in achieving high quality nanowires with low density of stacking faults because the nucleation probability of wurtzite (WZ)/zinc-blende (ZB) changes with the supersaturation of the catalysts.²³ Based on a nucleation-based model, WZ nucleation is favored at high supersaturation while ZB at low supersaturation.³³ Therefore, by further optimizing the III/V flux ratio, GaAsP nanowires with a low density of stacking faults can be obtained. Further investigation by line element mapping across the radial axis shows that the nanowire is uniform in composition (Figure 2c), which is evidence that the core–shell homojunction nanowire matches the lattice well. The energy-dispersive X-ray analysis along axial (Figure S3 and Table S1 of the Supporting Information) and radial axis (Figure S4 and Table S2 of the Supporting Information) also shows good composition uniformity of the homojunction nanowires. Figure 2d shows the photoluminescence spectrum of the GaAsP

homojunction nanowires measured at 300 K, where an emission peak at ~ 738 nm (1.68 eV) can be observed. Due to the large surface-to-volume ratio of nanowires, the high-density surface states usually act as nonradiative centers that degrade the optical property of nanowires. With a thin layer of InGaP passivation layer grown over the shell, the photoluminescence intensity is five times stronger than that of GaAsP nanowires without the passivation layer (Figure 2d). Figure 2e shows the integrated PL intensity as a function of temperature. The photoluminescence quenching shows a similar rate for nanowires both with and without InGaP passivation layer (Figure S5 and Table S3 of the Supporting Information). Over the entire temperature range, the InGaP passivated GaAsP nanowires show better photoluminescence than unpassivated GaAsP nanowires. Because of the large surface-to-volume ratio, surface states are considered the primary trapping centers for photoexcited carriers.³⁴ The enhanced photoluminescence of InGaP passivated GaAsP nanowires indicates a reduced density of surface trapping sites and an increased confinement for carriers after passivation.

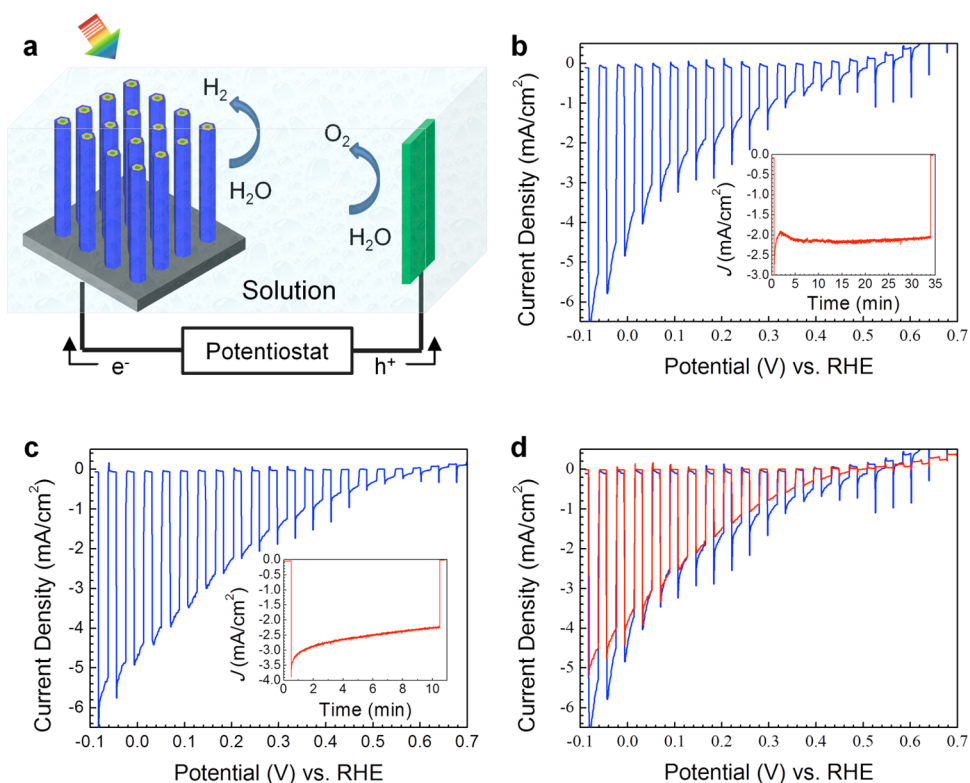


Figure 3. (a) PEC water splitting device structure for GaAsP nanowires grown on Si substrates. (b) Current density potential characteristics of GaAsP homojunction nanowires photocathode. (c) Current density potential characteristics of GaAsP homojunction nanowires photocathode with an InGaP passivation layer. (d) Comparison of the PEC performance between the GaAsP nanowire photocathode without InGaP passivation layer (blue line) and the one with passivation after stability test (red line). The insets in b and c are the steady-state current density of the photocathodes measured at 0.1 V versus RHE under AM 1.5G illumination. The current–potential curves were measured in 0.1 M KPi buffer solution (pH 7) at a scan rate of 10 mV/s under chopped AM 1.5G illumination.

The photoelectrochemical (PEC) performance of the nanowire photoelectrodes was measured with the three-electrode configuration with an Ag/AgCl reference electrode and a Pt wire counter electrode. A potentiostat (Hokuto Denko, HSV-100) was used to control the potential of the working electrode. The conversion of the measured potential (vs Ag/AgCl) to reversible hydrogen electrode (RHE) (NHE at pH = 0) was carried out by using the Nernst equation: $E_{\text{RHE}} = E_{\text{Ag/AgCl}} + 0.059 \text{ pH} + 0.197$. Before the PEC measurements, the nanowire photoelectrodes were modified with Pt nanoparticles as hydrogen evolution cocatalysts by photoassisted electrodeposition.^{35,36} The photoassisted electrodeposition was carried out in aqueous solution of 15 μM H_2PtCl_6 and 0.1 M Na_2SO_4 at pH 10. The potential of the nanowire photoelectrodes were kept at 0 V vs RHE under AM 1.5G illumination, and the electrodeposition was terminated until the saturation of the photocurrent. Both electrolytes of 0.1 M KPi (potassium phosphate) (pH = 7) and 0.1 M Na_2SO_4 (pH = 10) were used as the PEC reaction solution. An AM1.5 G solar simulator (SAN-EI Electric, XES-301 S) with an intensity of 100 mW/cm^2 was used to illuminate the photoelectrodes. The PEC properties of the GaAsP homojunction nanowire photocathode are shown in Figure 3. The InGaP passivated GaAsP nanowire photocathode is also given for comparison. The PEC properties of the GaAsP nanowire photocathode was characterized in a three-electrode setup with Ag/AgCl as the reference electrode, Pt as the counter electrode, and the GaAsP nanowire as the working electrode (Figure 3a). Figure 3b shows the current density–potential characteristics for the p–n

GaAsP homojunction nanowires photocathode under simulated air mass 1.5 global (AM 1.5G) solar illumination of 100 mW/cm^2 . Under AM 1.5G illumination, the photocurrent onset of the nanowires photocathode is at 0.54 V versus RHE. The high onset potential is attributed to an improved flat band potential caused by the band bending that is introduced by the p–n homojunction. The photocurrent density of the GaAsP nanowire photocathode is 4.5 mA/cm^2 at 0 V versus RHE. The current density is lower than planar III–V thin film based nanotextured photoelectrodes and selective area growth III–V nanowire photoelectrodes, due to low surface coverage and impeded carrier transport at the GaAsP/Si interface.^{13,32} The current density potential characteristics also show relatively low fill factors, which also suggests a poor interface between substrate and nanowires. However, this value is much higher than that reported for self-catalyzed III–V nanowires fabricated on a large scale.^{8,30} In addition, the GaAsP homojunction nanowires show a stable photocurrent for over 30 min for the steady-state photocurrent measurement as shown in the inset of Figure 3b. Figure 3c shows the PCE performance of the GaAsP nanowires with InGaP passivation layer. With the InGaP passivation layer, the photocurrent onset of the photocathode is increased to 0.63 V versus RHE. The improved onset potential suggests surface state passivation and superior carrier transport at the semiconductor–electrolyte interface.³⁰ The GaAsP nanowire photocathode with InGaP passivation layer also demonstrates a higher photocurrent density. The photocurrent density of the InGaP passivated photocathode is increased to 4.7 mA/cm^2 at 0 V versus RHE, and a higher photocurrent

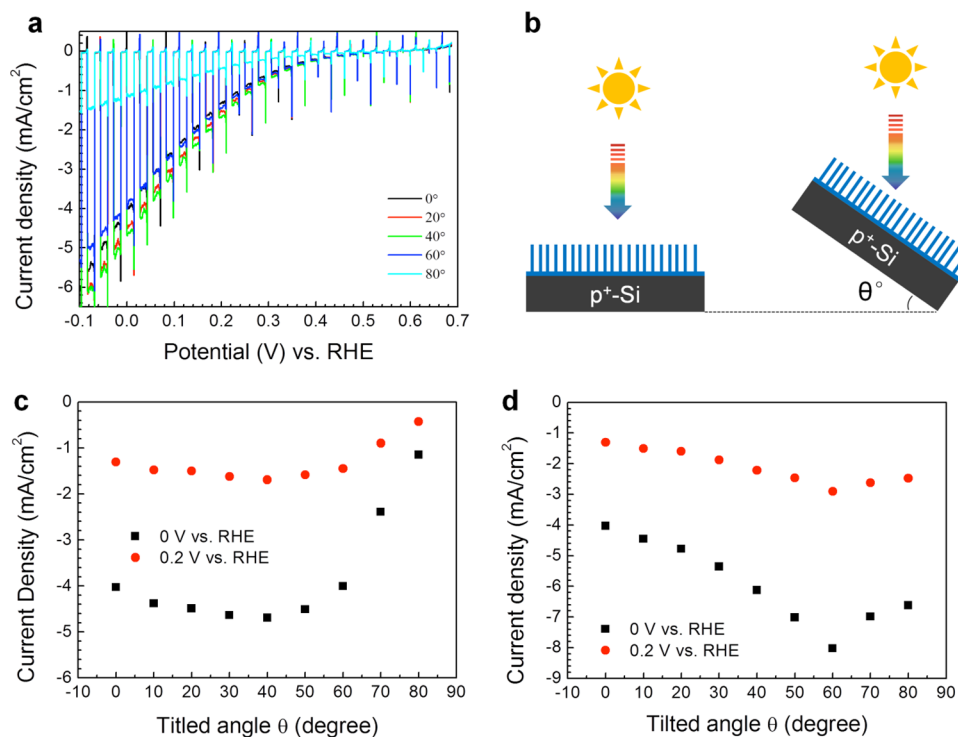


Figure 4. (a) Current density potential characteristics of GaAsP homojunction nanowires photocathodes with an InGaP passivation layer illuminated with normal incident light and off-normal incident light. The current–potential curves were measured in 0.1 M Na_2SO_4 solution (pH 10) at a scan rate of 10 mV/s under chopped AM 1.5G illumination. (b) Illustration of the illumination configuration during PEC performance characterization. (c) Current density measured 0 V vs RHE and 0.2 V vs RHE as a function of off-normal incident angle θ . (d) Current density in c normalized to the illumination area.

density is measured in the applied potential region between 0 to 0.6 V versus RHE. The improvement of photocurrent is also owing to reduced carrier recombination loss through surface trapping sites with InGaP passivation. Unfortunately, the InGaP passivation layer undergoes strong photochemical corrosion, and the photocurrent density decreases rapidly with time. At applied potential 0.1 V versus RHE, the current density is reduced from $\sim 3.5 \text{ mA/cm}^2$ to 2.5 mA/cm^2 in 10 min under AM 1.5G illumination. Figure 3d compares the PCE performance of the GaAsP nanowire photocathode with and without the InGaP passivation layer after a stability test. After the stability test, the PCE performance of InGaP passivated GaAsP nanowires photoelectrode is clearly degraded, and the on-set voltage and photocurrent density reach about the same level as the unpassivated GaAsP nanowire photoelectrode. Therefore, GaAsP is chemically more stable against photocorrosion than InGaP³⁷ and hence more suitable to be used as a photocathode.

It is worth noting that even though the nanowire density is as low as $1.8 \times 10^8 \text{ cm}^{-2}$, a good photocurrent density, $\sim 5 \text{ mA/cm}^2$ at 0 V vs RHE, has been measured. Considering the low surface fill factor of nanowires, many of the incoming photons are unabsorbed between the nanowires. Figure 4a compares the PEC performance of the nanowire photocathodes at different incident beam angles off the normal direction. As illustrated in Figure 4b, the substrates were tilted by an angle θ during the current potential measurements. The current density is increased from 4.0 mA/cm^2 to 4.7 mA/cm^2 at 0 V vs RHE when θ is increased from 0° to 40° (Figure 4c). Even though the photon flux is reduced by $\sim 23\%$ at the incident angle of 40° , the current density is about 17.5% higher than that measured with normal incident light. At 0.2 V vs RHE, the current density increased by about 30% from 1.3 mA/cm^2 to

1.7 mA/cm^2 (Figure 4c). At large angle θ , more photons can be absorbed by the nanowires despite the reduced photon flux. Moreover, in the vertical configuration of nanowires with a few micrometers in length, the photons are mainly absorbed at the upper part of the wires which can lead to a less efficient collection of holes. At off-normal incident illumination, the photon absorption in the nanowires is more evenly distributed and has a high collection efficiency for holes. Eventually, the current density starts to decrease when θ is $>40^\circ$ (Figure 4c). Figure 4d replots the normalized current density with photon flux as a function of θ . A maximum increase in current density from 4.0 mA/cm^2 to 8.0 mA/cm^2 at 0 V vs RHE is achieved at $\theta = 60^\circ$. When the applied potential is 0.2 V vs RHE, the increase in current density is more than doubled from 1.3 mA/cm^2 to 2.9 mA/cm^2 . Compared to the current density measured at normal incidence, the increase in current density is not offset by the reduction of photon flux until θ is as large as 70° , at which the photon flux is reduced by about 66%. The improved current density measured at reduced photon flux at off-normal incidence confirms that these GaAsP nanowires can have much better STH conversion capability than that measured from macroscale current density potential characteristics. Therefore, the STH conversion efficiency for GaAsP nanowire photoelectrodes could be significantly improved by increasing the absorption in the nanowires, such as an increase in the nanowire density. In addition to improvement in nanowire density, fabrication of single phase and twin free nanowires is also critical to achieve high photocurrent. Moreover, similar to nanowire solar cells, the nanowire geometry and spacing are also critical in achieving the optimum photocurrent density for photoelectrodes.^{38–40}

In conclusion, we have demonstrated the first 1.7 eV III–V nanowire photocathode monolithically grown on silicon substrates. Wafer-scale GaAsP homojunction nanowires have been fabricated through self-catalyzed approach. A STH conversion efficiency of 0.5% has been demonstrated for the GaAsP nanowire photocathode despite low surface coverage of the self-catalyzed nanowires ($\sim 1.8 \times 10^8 \text{ cm}^{-2}$). This STH conversion efficiency is higher than the values previously published for III–V nanowire photoelectrodes fabricated through self-catalyzed approach on a large-scale and could be significantly increased by further improving the density and material quality of GaAsP nanowires. This study paves the way for the development of low-cost and high-efficiency 1.7 eV/1.1 eV GaAsP/silicon tandem PEC cells.

■ ASSOCIATED CONTENT

Supporting Information

Photoluminescence mapping of core–shell GaAsP homojunction nanowires, nanowire density analysis, nanowire composition analysis, and temperature-dependent photoluminescence. This material is available free of charge via the Internet at <http://pubs.acs.org>.

■ AUTHOR INFORMATION

Corresponding Authors

*E-mail: jiang.wu@ucl.ac.uk.

*E-mail: yanboli@chemsyt.u-tokyo.ac.jp.

*E-mail: huiyun.liu@ucl.ac.uk.

Author Contributions

J.W. and Y.L. contributed equally to this work.

Notes

The authors declare no competing financial interest.

■ ACKNOWLEDGMENTS

H. Liu would like to thank The Royal Society for funding his University Research Fellowship.

■ REFERENCES

- (1) Kramer, G. J.; Haigh, M. *Nature* **2009**, *461*, 568–569.
- (2) Yehezkeili, O.; Tel-Vered, R.; Wasserman, J.; Trifonov, A.; Michaeli, D.; Nechushtai, R.; Willner, I. *Nat. Commun.* **2012**, *3*, 742.
- (3) Jeon, K.; Moon, H. R.; Ruminski, A. M.; Jiang, B.; Kisielowski, C.; Bardhan, R.; Urban, J. J. *Nat. Mater.* **2011**, *4*, 286–290.
- (4) Fujishima, A. *Nature* **1972**, *238*, 37–38.
- (5) Abdi, F. F.; Han, L.; Smets, A. H.; Zeman, M.; Dam, B.; van de Krol, R. *Nat. Commun.* **2013**, *4*, 2195.
- (6) Hou, Y.; Abrams, B. L.; Vesborg, P. C.; Björketun, M. E.; Herbst, K.; Bech, L.; Setti, A. M.; Damsgaard, C. D.; Pedersen, T.; Hansen, O. *Nat. Mater.* **2011**, *6*, 434–438.
- (7) Cho, I. S.; Lee, C. H.; Feng, Y.; Logar, M.; Rao, P. M.; Cai, L.; Kim, D. R.; Sinclair, R.; Zheng, X. *Nat. Commun.* **2013**, *4*, 1723.
- (8) Wang, D.; Pierre, A.; Kibria, M. G.; Cui, K.; Han, X.; Bevan, K. H.; Guo, H.; Paradis, S.; Hakima, A.; Mi, Z. *Nano Lett.* **2011**, *11*, 2353–2357.
- (9) Walter, M. G.; Warren, E. L.; McKone, J. R.; Boettcher, S. W.; Mi, Q.; Santori, E. A.; Lewis, N. S. *Chem. Rev.* **2010**, *11*, 6446–6473.
- (10) Chen, R.; Ye, Q.; He, T.; Ta, V. D.; Ying, Y.; Tay, Y. Y.; Wu, T.; Sun, H. *Nano Lett.* **2013**, *2*, 734–739.
- (11) Bolton, J. R.; Strickler, S. J.; Connolly, J. S. *Nature* **1985**, *315*, 6028, 495–500.
- (12) Chen, Y. W.; Prange, J. D.; Dühnen, S.; Park, Y.; Gunji, M.; Chidsey, C. E.; McIntyre, P. C. *Nat. Mater.* **2011**, *7*, 539–544.
- (13) Lee, M. H.; Takei, K.; Zhang, J.; Kapadia, R.; Zheng, M.; Chen, Y.; Nah, J.; Matthews, T. S.; Chueh, Y.; Ager, J. W. *Angew. Chem.* **2012**, *43*, 10918–10922.
- (14) Sun, K.; Pang, X.; Shen, S.; Qian, X.; Cheung, J. S.; Wang, D. *Nano Lett.* **2013**, *5*, 2064–2072.
- (15) Tian, B.; Kempa, T. J.; Lieber, C. M. *Chem. Soc. Rev.* **2009**, *38*, 16–24.
- (16) Holm, J. V.; Jørgensen, H. I.; Krogstrup, P.; Nygård, J.; Liu, H.; Aagesen, M. *Nat. Commun.* **2013**, *4*, 1498.
- (17) LaPierre, R. R. *J. Appl. Phys.* **2011**, *110*, 014310.
- (18) Kempa, T. J.; Day, R. W.; Kim, S. K.; Park, H. G.; Lieber, C. M. *Energy Environ. Sci.* **2013**, *6*, 719–733.
- (19) Dong, Y.; Tian, B.; Kempa, T. J.; Lieber, C. M. *Nano Lett.* **2009**, *9*, 2183–2187.
- (20) Gudiksen, M. S.; Lauthon, L. J.; Wang, J.; Smith, D. C.; Lieber, C. M. *Nature* **2002**, *415*, 617.
- (21) Lauthon, L. J.; Gudiksen, M. S.; Wang, D.; Lieber, C. M. *Nature* **2002**, *420*, 57.
- (22) Kargar, A.; Sun, K.; Jing, Y.; Chulmin, C.; Jeong, H.; Zhou, Y.; Madsen, K.; Naughton, P.; Jin, S.; Jung, G. Y.; Wang, D. *Nano Lett.* **2013**, *13*, 3017–3022.
- (23) Zhang, Y.; Aagesen, M.; Holm, J. V.; Jørgensen, H. I.; Wu, J.; Liu, H. *Nano Lett.* **2013**, *8*, 3897–3902.
- (24) Hong, S. J.; Lee, S.; Jang, J. S.; Lee, J. S. *Energy Environ. Sci.* **2011**, *5*, 1781–1787.
- (25) Zhang, L.; Fu, H.; Zhu, Y. *Adv. Funct. Mater.* **2008**, *15*, 2180–2189.
- (26) Kim, H. G.; Borse, P. H.; Choi, W.; Lee, J. S. *Angew. Chem.* **2005**, *29*, 4661–4665.
- (27) Seger, B.; Laursen, A. B.; Vesborg, P. C.; Pedersen, T.; Hansen, O.; Dahl, S.; Chorkendorff, I. *Angew. Chem., Int. Ed.* **2012**, *36*, 9128–9131.
- (28) Tian, B.; Kempa, T. J.; Lieber, C. M. *Chem. Soc. Rev.* **2009**, *38*, 16–24.
- (29) Tian, B.; Zheng, X.; Kempa, T. J.; Fang, Y.; Yu, N.; Yu, G.; Huang, J.; Lieber, C. M. *Nature* **2007**, *449*, 885–889.
- (30) Liu, C.; Sun, J.; Tang, J.; Yang, P. *Nano Lett.* **2012**, *10*, 5407–5411.
- (31) Shin, J. C.; Lee, A.; Katal Mohseni, P.; Kim, D. Y.; Yu, L.; Kim, J. H.; Kim, H. J.; Choi, W. J.; Wasserman, D.; Choi, K. J. *ACS Nano* **2013**, *7*, 5463–5471.
- (32) Hu, S.; Chi, C.; Fontaine, K. T.; Yao, M.; Atwater, H. A.; Dapkus, P. D.; Lewis, N. S.; Zhou, C. *Energy Environ. Sci.* **2013**, *6*, 1879.
- (33) Glas, F.; Harmand, J. C.; Patriarche, G. *Phys. Rev. Lett.* **2007**, *99*, 146101.
- (34) Joyce, H. J.; Gao, Q.; Hoe Tan, H.; Jagadish, C.; Kim, Y.; Zou, J.; Smith, L. M.; Jackson, H. E.; Yarrison-Rice, J. M.; Parkinson, P. *Prog. Quantum Electron.* **2011**, *2*, 23–75.
- (35) Dasgupta, N. P.; Liu, C.; Andrews, S.; Prinz, F. B.; Yang, P. J. *Am. Chem. Soc.* **2013**, *135*, 12932–12935.
- (36) Li, Y.; Zhang, L.; Torres-Pardo, A.; González-Calbet, J. M.; Ma, Y.; Oleynikov, P.; Terasaki, O.; Asahina, S.; Shima, M.; Cha, D.; Zhao, L.; Takane, K.; Kubota, J.; Domen, K. *Nat. Commun.* **2013**, *4*, 2566.
- (37) Khaselev, O.; Turner, J. A. *J. Electrochem. Soc.* **1998**, *145*, 3335–3339.
- (38) Kim, S. K.; Day, R. W.; Cahoon, J. F.; Kempa, T. J.; Song, K. D.; Park, H. G.; Lieber, C. M. *Nano Lett.* **2012**, *12*, 4971–4976.
- (39) Hu, Y.; Li, M.; He, J. J.; LaPierre, R. R. *Nanotechnology* **2013**, *24*, 065402.
- (40) Kempa, T. J.; Cahoon, J. F.; Kima, S. K.; Day, R. W.; Bell, D. C.; Park, H. G.; Lieber, C. M. *Proc. Natl. Acad. Sci. U.S.A.* **2012**, *109*, 1409–1412.